BIOCHEMISTRY
including biophysical chemistry & molecular biology

Article

pubs.acs.org/biochemistry

New Aspects of the Phosphatase VHZ Revealed by a High-Resolution Structure with Vanadate and Substrate Screening

Vyacheslav I. Kuznetsov, Alvan C. Hengge,* and Sean J. Johnson*

Department of Chemistry and Biochemistry, Utah State University, Logan, Utah 84322-0300, United States

Supporting Information

ABSTRACT: The recently discovered 150-residue human VHZ (VH1-related protein, Z member) is one of the smallest protein tyrosine phosphatases (PTPs) known and contains only the minimal structural elements common to all PTPs. We report a substrate screening analysis and a crystal structure of the VHZ complex with vanadate at 1.1 Å resolution, with a detailed structural comparison with other members of the protein tyrosine phosphatase family, including classical tyrosine-specific protein tyrosine phosphatases (PTPs) and dual-specificity phosphatases (DSPs). A screen with 360 phosphorylated peptides shows VHZ efficiently catalyzes the hydrolysis of phosphotyrosine (pY)-containing peptides but exhibits no activity toward phosphoserine (pS) or phosphothreonine (pT) peptides. The new structure reveals a deep and narrow active site more typical of the classical tyrosine-specific PTPs. Despite the high degrees of structural and sequence similarity between VHZ and classical PTPs, its general acid IPD-loop is most likely conformationally rigid, in contrast to the flexible WPD counterpart of classical PTPs. VHZ also lacks substrate recognition domains and other domains typically found on classical PTPs. It is therefore proposed that VHZ is more properly classified as an atypical PTP rather than an atypical DSP, as has been suggested.

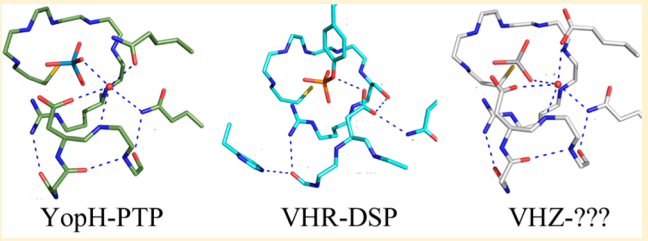

Protein tyrosine phosphatases (PTPs) are involved in multiple physiological processes, including cell growth and proliferation, control of the cell cycle, cytokine activation, and cytoskeletal integrity.[1,2] PTPs share the conserved signature HCXXGXXR(S/T) motif that binds the substrate and provides transition state stabilization, and a two-step catalytic mechanism with a cysteinyl−phosphate intermediate.[3−5] PTP family members are further subdivided into several subfamilies based on substrate specificity and sequence similarity. In vivo protein phosphorylation most commonly occurs on hydroxyl-containing aliphatic (serine/threonine) or aromatic (tyrosine) side chains, and the classical PTPs (often termed tyrosine-specific PTPs) hydrolyze only phosphotyrosine-containing polypeptides. The dual-specificity phosphatases (DSPs) constitute a subset of PTPs that are characterized by the ability to dephosphorylate phosphoserine and phosphothreonine residues in addition to phosphotyrosine.[6,7]

The active sites of all PTP family members are structurally similar and utilize an invariant triad of amino acids to catalyze phosphate monoester hydrolysis, which includes a nucleophilic cysteine; an arginine that, along with backbone amides, binds substrate and provides transition state stabilization; and an aspartic acid that protonates the leaving group. In the classical, tyrosine-specific PTPs, the latter catalytic residue resides on a flexible loop termed the WPD-loop.[8] In the DSPs, the general acid is believed to reside on a structurally rigid element.

Despite the high degree of structural similarity of catalytic domains, superimposable active sites, and a common mechanism, PTPs are selective for particular biological targets. The accurate identification of substrate preference and the correct assignment of these enzymes into the various PTP subfamilies associated with different biological pathways and pathological states are some of the most important goals of human phosphatome research. The recently discovered 150-residue human VHZ (also designated as atypical DSP 23) is one of the smallest PTP family members known to date, which contains only the minimal set of secondary structural elements common to all PTPs.[9−11] Because of its small size and the absence of substrate targeting domains, it has been classified as an atypical VH-1-related DSP,[11] a subfamily of cysteine-based PTPs that regulate mitogenic signaling pathways and cell cycle processes.[6,12] Atypical DSPs have been linked to cancer, but despite numerous studies, knowledge of these enzymes still remains contradictory and incomplete.[13,14] Attempts to identify the physiological substrates of VHZ have provided conflicting and inconsistent evidence.[9,15,16] It is known, however, that VHZ is highly expressed in fetal tissues, and recent reports have associated VHZ with breast cancer.[17]

The only crystal structure of VHZ published to date is a complex with malate trapped in the active site.[18] Malate ion is an important part of VHZ crystallization conditions but represents neither a substrate nor a product analogue. Potential resulting distortions in the local geometry of the active site motivated us to seek a structure with a physiologically relevant reaction analogue. We report a high-resolution X-ray structure of VHZ complexed

Received: July 6, 2012
Revised: November 8, 2012
Published: November 12, 2012

with the physiologically relevant transition state analogue metavanadate that allows us to compare VHZ structurally with a number of classical PTP and atypical DSP protein−ligand complexes. This analysis suggests that VHZ bears more resemblance to the classical PTPs rather than DSPs but probably lacks a movable loop. These conclusions from the crystal structure support the results of a phosphopeptide substrate screen, which revealed that phosphotyrosine-containing peptides, but not phosphoserine- or phosphothreonine-containing peptides, are substrates for VHZ. The collected results strongly suggest that VHZ is more related to the classical PTPs rather than the atypical DSP subfamily, and to more properly guide future research in the biological roles of VHZ, its current classification should be reconsidered.

EXPERIMENTAL PROCEDURES

Materials and Methods. All buffer solids, EDTA, malic acid, ammonium sulfate, and sodium orthovanadate were obtained from Fisher. Chromatography columns were purchased from GE Healthcare. Protease K was from Sigma. Polyethyleneimine (M_w = 50000) was from Acros Organics. A set of standard FastDigest restriction enzymes, DNA Pfu Turbo Polymerase, and dNTP master mix were obtained from Fermentas. Custom primer oligonucleotides were synthesized by IDT. The phosphatase substrate screen was from GPT Innovative Peptide Solution. DTT, antibiotics, and protease inhibitors were from GoldBio.

Protein Cloning. The human VHZ wild-type (WT) gene was amplified using a two-step polymerase chain reaction (PCR) strategy from a GST-tagged version on a plasmid that was a generous gift from S. Swaminathan.[18] In the first step, the gene was amplified using primers Fwd1 (**GAAAACCTGTATTTTCAGGGC**GTGCAGCCCCCC) and Rev1 (GGA**GAGCTC**TTATTTCGTTCGCTGGTAGA) to incorporate the TEV cleavage site (in bold) immediately upstream of the first N-terminal GGC codon (methionine excluded). At the same time, a SacI restriction site (GAGCTC, in bold) was added at the end of the sequence. In the second PCR step, the product of the first step was used as a template and a KpnI restriction site was added upstream of the TEV protease cleavage sequence using the following set of primers: Fwd2, CGG**GGTACC**GAAAACCTGTAT; Rev1, GGAGAGCTCTTATTTCGTTCGCTGGTAGA. The PCR product was digested with KpnI and SacI restriction enzymes (Fermentas) and inserted into the pet-45(B+) vector (Novagen). The obtained pet 45B+TEV-VHZ construct was successfully expressed in BL21-codon+(DE3)-RIL cells and purified with Ni-Fast Flow high-affinity resin (GE Healthcare). Unfortunately, the resulting fusion protein was resistant to TEV cleavage of the polyhistidine tag, and the tagged protein was unstable at low pH. Insertion of a short spacer arm following the histidine tag did not improve TEV cleavage.[19] A tagless enzyme construct was prepared by removal of the histidine tag and TEV cleavage site from the pET 45b-TEV-VHZ construct using one-step overlap extension PCR[20] using the following primers: Fwd, TATACCATGGGCGTGCAGCCC; Rev, CGTGCACGCCCATGGTATATCT. The resulting construct was used to express tagless VHZ WT in BL-21 DE-3 (codon+) cells.

Protein Preparation. Tagless VHZ WT was expressed in BL21-codon+(DE3)-RIL cells. The cells were grown at 37 °C to an OD_{600} of 1.2−1.5. Protein expression was induced with IPTG (100 mg/L), and cell culture flasks were transferred to a room-temperature shaker for 20 h before cells were harvested. The cells were harvested by centrifugation for 15 min and resuspended in lysis buffer containing 50 mM HEPES, 150 mM NaCl, 1 mM EDTA, 10 mM DTT, and 5% glycerol (pH 7.4) at 4 °C. Cells were disrupted by sonication on ice, and the pellet was separated by centrifugation. The supernatant was transferred into a separate beaker, and a 10% (w/v) solution of polyethyleneimine (PEI, M_w = 50000, pH 8.0) was added dropwise to the supernatant at 4 °C to yield a final PEI concentration of 0.5% (w/v). White precipitate formed immediately and was separated by centrifugation. Ammonium sulfate was added to the supernatant (to 65% saturation), and precipitated protein was collected and resuspended in 150 mL of SP-loading buffer containing 100 mM sodium acetate, 1 mM DTT, 1 mM EDTA, and 10% glycerol (pH 5.6). The solution was filtered, and 15 mL of Hi-Trap SP-HP cation exchange resin (GE Healthcare) pre-equilibrated with SP-loading buffer was added to the protein (4 °C). The resin was transferred into a column and washed with SP-loading buffer (2 mL/min) to reach a stable baseline. Protein was eluted using a 120 mL linear gradient with elution buffer containing 100 mM sodium acetate, 1 mM DTT, 1 mM EDTA, 600 mM sodium chloride, and 10% glycerol (pH 5.6). Fractions containing phosphatase activity toward *p*-nitrophenyl phosphate (*p*NPP) were collected, concentrated to a volume of 3−5 mL, and loaded on a Superdex 75 26/60 gel filtration column (GE Healthcare) pre-equilibrated with buffer containing 10 mM HEPES, 150 mM NaCl, 1 mM methionine, 3 mm DTT, and 10% glycerol (pH 7.5) at 4 °C and 0.3 mL/min. The single peak corresponding to VHZ WT was collected and estimated to be >98% pure based on the sodium dodecyl sulfate−polyacrylamide gel electrophoresis analysis. The protein was concentrated to 20 mg/mL as determined by UV using an $A^{280}{}_{1\ mg/mL}$ of 0.68.

Determination of Substrate Specificity. The commercial phosphopeptide screen from JPT Innovative Peptide Technologies (product no. PhSS-360-250) was used. The full list of phosphopeptides comprising this screen is available at the manufacturer's website (http://jpt.com) and is included in Table S1 of the Supporting Information. Twenty-five microliters of buffer containing 100 mM sodium acetate, 0.5 mM DTT, 150 mM NaCl (pH 5.5), and 0.25 unit of VHZ WT (0.55 mg/mL) was added to each well of a 384-well microtiter plate containing 360 phosphopeptides (250 pmol/well) derived from human phosphorylation sites together with 10 calibration standards. After incubation for 2 h at 25 °C, 5 μL of protease K (Sigma, 200 μg/mL) was added to digest the enzyme and prevent enzyme precipitation after addition of the malachite green reagent. After 15 min, 30 μL of the malachite green solution (Promega) was added and color developed for 10 min. The absorbance at 650 nm was measured to quantify the amount of free inorganic phosphate released by the enzyme using a standard curve. This was converted to a percent of total hydrolysis using the supplier-provided information for the amounts of substrate in each well. Subsequently, k_{cat} and K_M were measured for two peptide substrates, one that exhibited among the highest percent of hydrolysis (QREAEpYEPETV) and one from the group exhibiting the least (DADEpYLIPQQG). In a control experiment, incubation of pY-containing peptides under the assay conditions without enzyme exhibited no measurable hydrolysis after 48 h.

Cocrystallization with Sodium Vanadate. All crystallization experiments were conducted at room temperature using the sitting drop vapor diffusion method. VHZ WT concentrated to 20 mg/mL in the crystallization buffer was mixed with a 50 mM solution of sodium vanadate (final vanadate concentration of 10 mM; K_i = 2.7 μM) prepared as previously described.[21] One

microliter of the protein−vanadate complex was mixed with an equal volume of a well solution containing 150 mM L-malate (pH 7.0) and PEG3350 (15−20%). A 1 M stock solution of sodium malate was prepared by titration of malic acid with sodium hydroxide. Crystals grew within 1 week.

Data Collection and Processing. The crystal in the droplet was transferred to a cryosolution containing the well solution supplemented with 10% (v/v) glycerol and 10 mM sodium vanadate for 10 min and flash-frozen in liquid nitrogen. Diffraction data were collected at the Stanford Synchrotron Radiation Lightsource (SSRL) on beamline 9-2. The collection and refinement statistics are listed in Table 1. Molecular replacement was performed with Phenix[22] using the previously published VHZ structure [Protein Data Bank (PDB) entry 2IMG] as a search model with malate ion in the active site removed. Coot[23] and MolProbity[24] were used for model building and validation. Phenix was used for model refinement. PyMol[25] was used to prepare figures and superimpose structures. Structure factors and coordinates have been deposited in the Protein Data Bank as entry 4ERC.

Table 1. Data Collection and Refinement Statistics for VHZ with VO_3

Data Collection	
beamline	9-2 at SSRL
wavelength (Å)	0.97946
resolution range (outer shell) (Å)	50.00−1.15 (1.19−1.15)
no. of reflections	
unique	94449
total	1237514
average redundancy	13.1 (12.2)
mean $I/\sigma(I)$	31.3 (3.8)
completeness (%)	99.6 (99.4)
R_{sym} (%)	6.8 (66.6)
space group	$P2_12_12_1$
unit cell dimensions	a = 33.0 Å, b = 79.9 Å, c = 99.7 Å, $\alpha = \beta = \gamma = 90°$
Refinement	
R_{work}, R_{free} (%)	12.8, 14.5
no. of atoms in the structure	5312
protein	4838
water	466
ligand/ion	8
average B factor (Å^2)	
protein	13.6
water	26.6
rmsd for bonds (Å), angles (deg)	0.008, 1.245
protein geometry	
Ramachandran favored (%)	96.07
Ramachandran outliers (%)	0.66
rotamer outliers (%)	1.57
Protein Data Bank entry	4ERC

RESULTS

Substrate Specificity of VHZ. The substrate specificity of VHZ was assessed using a phosphatase substrate set containing 360 peptides, corresponding to natural in vivo phosphorylation sites monophosphorylated on serine, threonine, or tyrosine. Amino acids adjacent to the phosphorylation site play an important role in recognition of the substrate by different PTPs.[26] The structural diversity of the JPT screen accounts for potential bias resulting from adverse binding effects caused by unfavorable amino acids proximal to the phosphorylated site, and thus allows a reliable assessment of the comparative effectiveness of VHZ in catalyzing the hydrolysis of pS-, pT-, and pY-containing peptides. Because the goal of this experiment was to determine whether VHZ was a DSP or a PTP, reaction mixtures were given a sufficiently long time to incubate before they were assayed to ensure that even substrates yielding very low activity would be detected. After 2 h, enzymatic activity was observed in every well containing a pY-phosphorylated peptide, with an average hydrolysis of 50−60%. No activity was observed in wells containing either pS- or pT-phosphorylated peptides. In particular, no activity was observed in the wells containing serine/threonine monophosphorylated peptides corresponding to the previously tested MBP (myelin binding protein) and common DSP substrates containing the TXY activation loop of MAPK8—MAPK11. The peptide sequences that yielded greater than average levels of hydrolysis are listed in Table S2 of the Supporting Information. In subsequent experiments, k_{cat} and K_M were determined for the QREAEpYEPETV substrate, one of the substrates exhibiting the highest percent of hydrolysis, and for DADEpYLIPQQG, which was among those that exhibited the lowest activity. These kinetic results are listed in Table 2.

General Structure Description. The crystal structure of VHZ complexed with metavanadate was determined to 1.1 Å resolution (Figure 1). The structure was refined to R_{work} and R_{free} values of 12.8 and 14.5%, respectively (Table 1). Two molecules of VHZ are contained in the asymmetric unit. The final model includes protein residues 1−150 and a metavanadate (VO_3) ligand present in each active site. VHZ is a single-domain protein consisting of a central, twisted, five-stranded β-sheet surrounded by six α-helices, two on one side and four on the other (Figure 1). The conserved phosphate-binding loop (P-loop) connects strand β5 and helix α4, and the general acid loop (termed the IPD-loop[11] by analogy to the conserved WPD-loop of the classical PTPs) connects elements α3 and β4. The D residue of the IPD motif (D65) acts as the general acid during catalysis. The Q-loop (connecting α6 and α5) further defines the active site cleft. The overall VHZ structure represents a typical one for the PTP family α/β-domain. Both molecules in the asymmetric unit adopt a similar protein conformation. The guanidinium side chains of R60 and R62 from the symmetry-related VHZ molecule are observed in the area of the active sites of molecules A and B, respectively (Figure 2A,C).

Comparison with the Structure of the VHZ−Malate Complex. The structure of the VHZ−VO_3 transition state complex differs in several important ways from that of the

Table 2. Kinetic Constants for the Hydrolysis of Two Substrates Selected from the Substrate Screen

peptide sequence	k_{cat} (s^{-1})	K_M (mM)	k_{cat}/K_M ($\times 10^{-3}$ M^{-1} s^{-1})	% hydrolysis[a]
QREAEpYEPETV	0.56 ± 0.02	1.9 ± 0.2	0.3	100
DADEpYLIPQQG	0.53 ± 0.06	4.2 ± 0.4	0.12	50

[a]Percent of hydrolysis observed in the long time course general substrate screen.

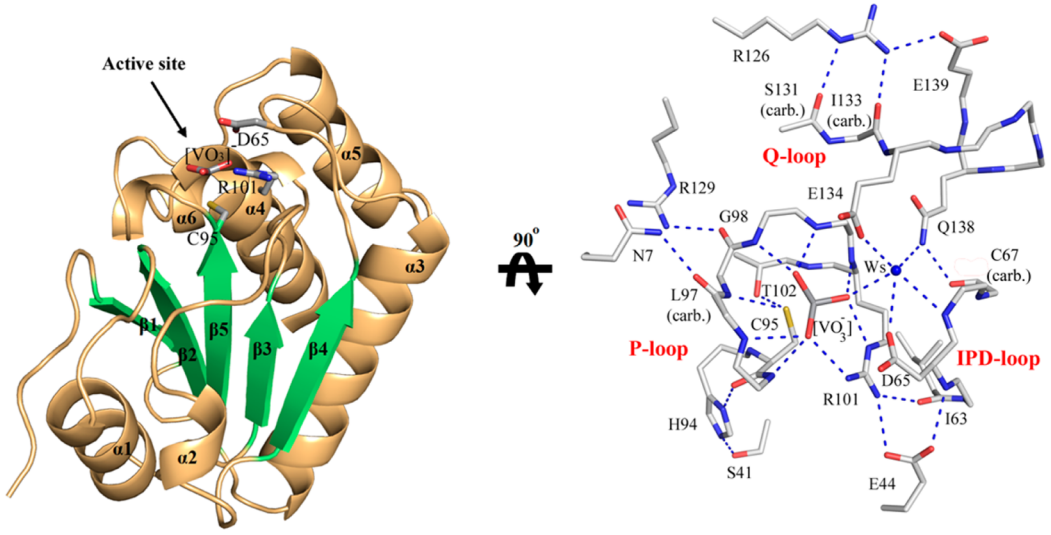

Figure 1. Structure of the VHZ–VO_3 complex. The cartoon representation of the VHZ–VO_3 structure reveals a classical PTP α/β-fold with a central region composed of a β-sheet (green) surrounded by α-helices (brown). The important active site residues and hydrogen bond network (dashed lines) surrounding the VO_3 oxyanion are shown.

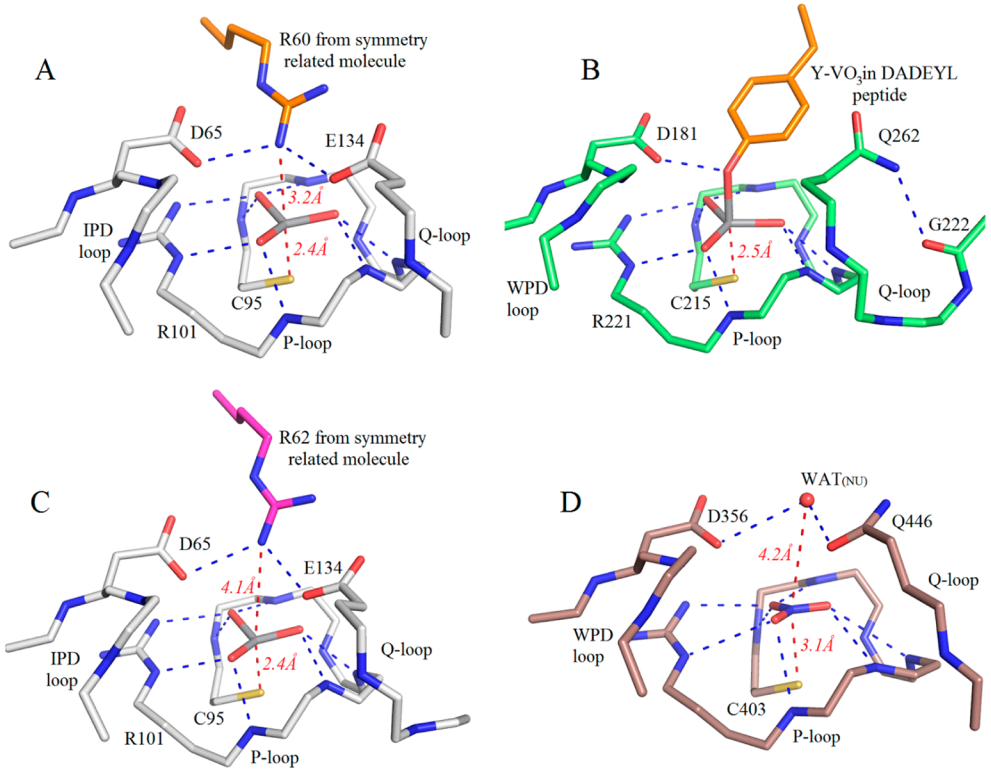

Figure 2. Comparison of the VHZ–VO_3 complex with analogous PTP1B structures. (A) VO_3 molecule at the VHZ active site in chain A coordinated by P-loop hydrogen bonds. The structural water shown in Figure 1 has been omitted for the sake of clarity. Hydrogen bond distances (red) are in angstroms. The vanadium–sulfur distance is similar to that observed in PTP1B structure PDB entry 3I7Z (B) with a bound vanadyl peptide. The R60 side chain belongs to the symmetry-related VHZ molecule trapped near the active site. (B) Transition state analogue structure for the first catalytic step of PTP1B (PDB entry 3I7Z), consisting of the enzyme bound to the tyrosyl vanadyl ester of the DADEYL peptide. (C) VO_3 moiety at the VHZ active site in chain B. (D) Crystal structure of YopH with nitrate bound, taken as a transition state analogue for the second catalytic step of the PTP mechanism (PDB entry 1YPT). The R62 side chain nitrogen atom from a symmetry-related VHZ molecule near the active site in chain B in panel C assumes a position that is analogous to that of the nucleophilic water molecule [$WAT_{(NU)}$].

previously published VHZ–malate complex. In the VHZ–Mal structure, the malate ion makes four hydrogen bonds to the backbone of the P-loop, two hydrogen bonds to the side chain of R101, and one hydrogen bond to the backbone of the IPD-loop. The catalytic acid D65 (in the IPD-loop) and E134 (in the Q-loop) are turned away from the active site (presumably repelled by the negative charge of the malate carboxylate groups). As a result, the IPD-loop adopts a catalytically unfavorable conformation in which D65 hydrogen bonds to the side chain of the conserved phosphate-binding residue R101. Additionally, this

dx.doi.org/10.1021/bi300908y | *Biochemistry* 2012, 51, 9869–9879

catalytically unviable conformation imparted by malate distorts the VHZ active site into a shallow and broad crevice reminiscent of DSPs. In the VHZ−Mal complex, the side chain of Y136 from the symmetry-related molecule is trapped in the active site, which, together with the rest of the molecule, makes five additional crystal contacts in the area of the active site, further complicating the interpretation of this structure.

In the structure of the VHZ−VO_3 complex, the active site contains a region of distinct electon density corresponding to a low-*B* factor water molecule. The water is located whithin hydrogen bonding distance of the equatorial oxygens of VO_3, the side chains of E134 (Q-loop), Q138 (Q-loop), and D65 (IPD-loop), and the backbone amide nitrogen of F66 (Figure 1). It is absent in the VHZ−Mal structure because of interactions of the malate ion, but a water in this position is consistently observed in X-ray structures of classical PTPs such as *Yersinia* PTP and PTP1B. It represents an important node coordinating the primary active site elements in classical PTPs but not in VH1-related DSPs (Figure 4A,B).

The VHZ−VO_3 complex (Figure 2) reveals the active site arrangement observed in many classical PTP structures in which all of the catalytic elements are properly positioned for catalysis. The electron density in the active site region clearly reveals the $[VO_3]^-$ ion is coordinated in each active site to the P-loop amide backbone as well as to the side chain of R101. The sulfur of C95 is 2.4 Å from the central vanadium atom. The electron density indicates 100% occupancy of the $[VO_3]^-$ ion bound to one of the VHZ molecules (chain A) but only 86% occupancy in the second molecule (chain B). The guanidinium moiety of R101 makes bidentate hydrogen bonds with the bound metavanadate, which is a transition state analogue of the transferring phosphoryl group. The general acid D65 is located in a position suitable for protonation of the scissile oxygen atom, as is commonly observed in similar ligand-containing PTP structures. The nucleophilic cysteine sulfur atom is in an apical position relative to the central VO_3 moiety.

Interestingly, a gap in electron density exists between the C95 and the vanadate in both the $2F_o - F_c$ difference map and in an unbiased composite omit map (Figure 3A,C). Modeling and refinement of a covalently bound cysteinyl−vanadate adduct resulted in a large negative electron density peak in the region between the sulfur and vanadium (Figure 3B), whereas relaxation of the geometry constraints during refinement yielded the original model with a noncovalent sulfur−vanadium interaction. This suggests a primarily electrostatic interaction rather than a covalent bond between cysteine 95 and the vanadium atom, which has been confirmed by a computational analysis.[27]

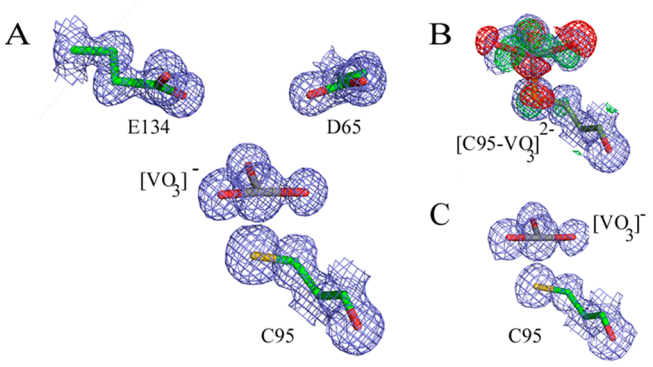

Figure 3. Electron density at the VHZ active site reveals a noncovalently bound vanadate molecule. (A) $2F_o - F_c$ (blue) maps contoured at 1.5σ around catalytic C95, metavanadate, and neighboring residues in the refined model. The arginine from the symmetry-related molecule was omitted for the sake of clarity. (B) $2F_o - F_c$ (1.5σ) (blue) and $F_o - F_c$ (±3.0σ) maps (green for positive, red for negative) produced after refinement with a covalently bound cysteinyl−vanadate model. (C) Unbiased composite omit map contoured at 1.5σ in the same orientation as in panel A.

Functional Analysis of the VHZ Active Site. The active site of classical PTPs is formed by the phosphate-binding loop (P-loop), a glutamine-bearing loop (Q-loop), a general acid loop (WPD-loop), and a substrate-binding (recognition) loop. VHZ lacks a substrate recognition loop, which is normally located at the N- terminus of classical PTPs. These loop regions in VHZ, compared with those of PTPs and DSPs, are discussed separately.

P-Loop Interactions (VHZ residues 95−102). The P-loop interactions with bound VO_3 in VHZ are presented in Figure 1. The backbone amides of five P-loop residues make hydrogen bonds to the $[VO_3]^-$ ion. The amide of conserved G98 makes a catalytically important hydrogen bond to the side chain of the nucleophilic C95.[28] The side chain of T102 also donates a hydrogen bond to the C95 sulfur, assisting the breakdown of the phosphoenzyme intermediate in the second step of the overall reaction, another conserved feature of the PTP family.[29] The carbonyl oxygen of G98 makes a hydrogen bond to the side chain of R129, which, together with the side chain of N7, provides conformational stability to the P-loop. This arginine is highly conserved in all PTPs, and mutation leads to the loss of enzymatic activity.[30] In atypical DSPs, in addition to the structural role, this residue is important for the recognition of bisphosphorylated peptide substrates, providing a positive charge in the second docking site on the protein surface.[30] In classical PTPs, this arginine is shielded from the surface by protein structural elements and plays no role in substrate recognition. In VHZ, as in classical PTPs, R129 is shielded from the surface by the side chain of N7 (Figure 1). The guanidinium R101 side chain, which binds the phosphate moiety of the substrate, makes two hydrogen bonds to the metavanadate equatorial oxygens, the carbonyl oxygen of I63 (in the IPD-loop) and the carboxyl oxygen of E44.

Q-Loop Interactions (residues 127−138). In classical PTPs, this region is characterized by two conserved Q residues and participates in catalysis by the activation and orientation of the nucleophilic water in the second step.[31,32] Important Q-loop interactions are presented in Figure 1. The Q-loop motif in VHZ is identical to that in classical PTPs with exception of the substitution of the first Q with E, which, however, resulted in no functional changes in YopH.[32] The side chains of E134 and Q138 are directed toward the active site and together with D65 (from the IPD-loop) serve to position the incoming nucleophilic water. The analogous N-loop region in atypical DSPs (Figure 4) is positioned such that it provides a broad and shallow active site opening required for dual specificity that has no conserved glutamines.

IPD-Loop Interactions (residues 61−71). The general acid loop in VHZ has been termed the IPD-loop, by analogy with the conserved WPD-loop in the classical PTPs.[18] This loop carries the D65 general acid that protonates the leaving group in the first step and acts as a general base in the second step activating the nucleophilic water.[16,33,34] The interactions involving IPD-loop residues are shown in Figures 1 and 2. The IPD-loop position corresponds with the closed, catalytically active position of the WPD-loops in classical PTPs. The side chain of I63 docks in a hydrophobic pocket created by the aliphatic part of R101 and the

dx.doi.org/10.1021/bi300908y | *Biochemistry* 2012, 51, 9869−9879

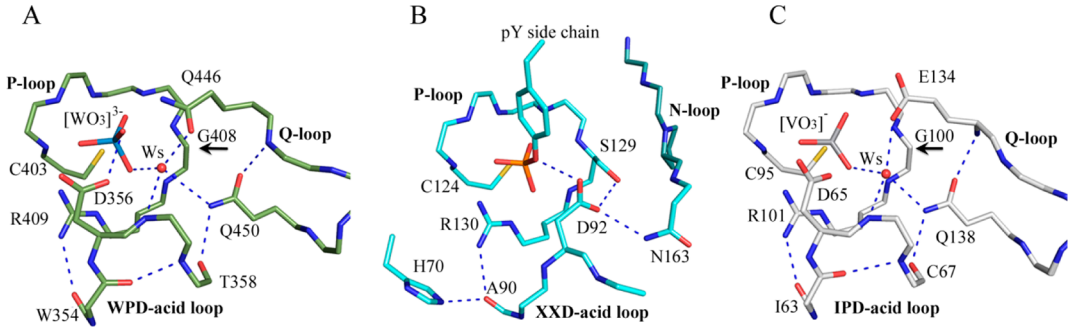

Figure 4. Important distinctions between atypical DSPs and classical PTPs. The catalytic general acids are D356, D92, and D65 in YopH, VHR, and VHZ, respectively; all structures are viewed at the same angle in relation to the structurally superimposable P-loop. The topology and hydrogen bond network of the general acid loop and Q-loop in YopH−1YTW (A), VHR−1J4X (B), and VHZ−VO_3 (C) complexes reveal important distinctions between classical PTPs (represented by YopH) and atypical DSPs (represented by VHR): (1) Stabilization of the general acid WPD-loop in classical PTPs (A) and atypical DSPs (B) is obviously different. In particular, the structural water (W) provides stabilization to the general acid loop in YopH and VHZ but is never observed in atypical DSPs. In VHR (and other atypical DSPs), the general acid loop is stabilized by the cluster of highly conserved serine/asparagine residues [S129/N163 in VHR (B)]. As a result, the position of the general aspartic acid in PTPs and DSPs is different and the leaving group protonation occurs at different angles. (2) Classical PTPs use invariant Q-loop residues [Q446 and Q450 (A)] to orient the incoming nucleophilic water (not shown in the figures). The analogous E134 and Q138 residues are present in VHZ (C). The analogous region in VHR, named the N-loop, has no analogous residues and bears the invariant structural asparagine [N163 (B)]. (3) The glycine residue in YopH [G408 (A)] and VHZ [G100 (C)] provides the important access of Q446 and E134 to the active site, whereas the invariant structural serine is present in VHR [S129 (B)] and other atypical DSPs.

side chains of M105, V93, and P69, providing hydrophobic interactions similar to those involving the conserved W in classical PTPs.[35] Similar to clasical PTPs, the carbonyl oxygen of I63 makes a hydrogen bond to R101, retaining its side chain in the catalyticaly favorable substrate binding conformation. Additional hydrogen bonds occur between the carboxyl oxygen of D65 and structural water W_S as well as between the carbonyl oxygen of C67 and the side chain nitrogen of Q138. Such interactions are characteristic of the WPD-loop stabilization in classical PTPs (Figure 4A) but not in atypical DSPs (Figure 4B).[36] The structural water molecule is absent in all atypical DSP structures reported to date. Instead, general acid positioning is provided by the side chain of a conserved asparagine from the N-loop motif and the conserved serine from the P-loop. As the result, the general acid position in relation to the leaving group differs in PTPs compared to DSPs, and protonation occurs from different angles (Figure 4A,B).

Sequence Analysis of VHZ. With the goal of ascertaining where VHZ fits in the PTP−DSP continuum, we compared the sequences and structures of VHZ and several classical PTPs and VH1-related DSPs. Because of significant size differences and little conservation outside of the following regions, alignments were confined to the general acid loop, P-loop, and Q-loop as the three most important catalytic regions. The results, shown in panels A and B of Figure 1S of the Supporting Information, reveal both the significant resemblance of VHZ to the classical PTPs and important distinctions from atypical DSPs.

Sequence Analysis of the P-Loop. The general PTP family signature motif (P-loop motif) contains the HCXXGXXR(S/T) sequence.[1,37] As can be seen from the sequence alignments in panels A and B of Figure 1S of the Supporting Information, the conserved motif in classical PTPs is HCXXGX**G**RT whereas in atypical DSPs this sequence is HCXXGX**S**RS. Position H + 6 (bold) is exclusively occupied by glycine in classical PTPs and by serine in atypical DSPs. The serine at this position in atypical DSPs donates a hydrogen bond to the general acid (Figure 4B), contributing to its correct positioning for catalysis. Mutation of S129 to G in VHR abolishes general acid catalysis by D92 (data not shown). In classical PTPs, glycine occupies the analogous position (Figure 4A), which permits conserved Q-loop glutamine residues (Q446 and Q450 in YopH) to access the active site and participate in the second step of the reaction by positioning the nucleophilic water.[32,38] VHZ (Figure 4C) resembles classical PTPs in having glycine (G100) rather than serine at this position, which allows the E134 side chain to access the active site.

Sequence Analysis of the Q-Loop. In classical PTPs (Figure 1SA of the Supporting Information), this region contains the (V/I)**Q**(R/T)XX**Q** motif. The region is named after two catalytically important Q residues that serve to orient and activate the nucleophilic water molecule in the second step.[32,38] The corresponding N-loop in atypical DSPs characterized by the highly conserved PNXXFXXQL sequence contains a conserved asparagine residue (N163 in VHR), which together with the conserved S residue in the P-loop (S129 in VHR) donates a hydrogen bond to the general acid and stabilizes its catalytically favorable conformation (Figure 4B).

Sequence Analysis of the IPD-Loop. In the atypical DSPs, the general acid-bearing loop has no sequence conservation (Figure 1SB of the Supporting Information) with the exception of the catalytic aspartic acid and, unlike the WPD-loop, does not undergo conformational changes.[36] The sequence alignment of VHZ with classical PTPs (Figure 1SA of the Supporting Information) shows its IPD-loop is highly analogous to the WPD-loop in classical PTPs with the exception of I63 in place of the conserved W. The MOTIF server was used to search the RSCB database for structures that simultaneously contain the PTP family HCXXXXR[S/T] motif and a variable general acid XXDXXP loop region (Figure 1SC of the Supporting Information) but not the highly conserved PNXXXF N-loop sequence, thus allowing us to eliminate atypical DSPs. The goal was to identify proteins that, like VHZ, are related to classical PTPs but with variability of the general acid loop region. Alignment of the retrieved structures [e.g., VSP (3AWF), PTEN (1D5R), KAP1 (1FPZ), PhyA (3F41), SsoPTP (2I6I), and CDC14B (1OHC)] revealed the common PTP α/β-fold with general acid XXD-loops that can be superimposed with the IPD-loop in VHZ and the WPD-loop in classical PTPs (Figure 1SC of

dx.doi.org/10.1021/bi300908y | *Biochemistry* 2012, 51, 9869−9879

the Supporting Information). These proteins share the active site architecture of classical PTPs with substitutions for W in the general acid loop. On the basis of the sequence alignment analysis and structural and functional information about the retrieved proteins, VHZ is most closely related to *Sulfolobus solfataricus* rather than VSP, PTEN, KAP1, PhyA, or CDC14B.

DISCUSSION

Identification of VHZ Substrate Specificity. The substrate specificity of VHZ has been the subject of several conflicting studies. In one study, VHZ was found to effectively dephosphorylate ERK, but not JNK or p38.[10] In another study, VHZ was found to effect JNK and p38 with no apparent effect on ERK.[9] These substrates are common ones among DSPs. The substrate screen used in this study contained several sequences corresponding to activation loops of MAPK8, MAPK9, MAPK10, and ERK1 monophosphorylated at pT or pS. No activity was detected in these wells, indicating that if VHZ targets the reported proteins, it may dephosphorylate only the phosphotyrosine of the pTXpY activation loops, unlike the DSP VHR, which targets both sites.[30] The observed dephosphorylation pattern is characteristic of classical tyrosine-specific PTPs, which result in monophosphorylated MAPK forms and retain reduced but significant activity compared to the biphosphorylated proteins.[39] DSPs have a preference, but not specificity for, bisphosphorylated substrates and have the ability to act on singly phosphorylated pS and pT peptides. As described above, because R129 is shielded by the side chain of N7, it is unlikely that VHZ has a preference for bisphosphorylated substrates.[30,40] These results suggest that VHZ is a phosphotyrosine-specific PTP rather than a DSP.

Two substrates, one from among those showing the highest hydrolysis percentage and one showing the lowest, were chosen for more detailed kinetic analysis. Table 2 shows the k_{cat}, K_M, and k_{cat}/K_M for the QREAEpYEPETV and DADEpYLIPQQG substrates. The substrates have different K_M but similar k_{cat} values. The k_{cat} values are higher than a reported k_{cat} of 0.009 s^{-1} with pNPP.[11] Related enzymes (VH1, VHX, and VHY) show k_{cat} values in the range of 0.2−0.9 s^{-1} with *p*NPP.[11] The substrate DADEpYLIPQQG has also been tested with YopH and PTP1B. At pH 6.6 and 30 °C with YopH, $k_{cat} = 1314 \pm 18$ s^{-1} and $K_M = 59 \pm 4$ μM; with PTP1B, $k_{cat} = 75.7 \pm 1.0$ s^{-1} and $K_M = 2.63 \pm 0.37$ μM.[41] Both YopH and PTP1B exhibit very similar k_{cat} values for a range of phosphopeptide substrates regardless of sequence. The same trend is apparent in these two VHZ substrates, where the difference in hydrolysis arises from K_M rather than k_{cat}. Such consistency in turnover number is a common feature of PTPs, although k_{cat} varies over several orders of magnitude among enzymes within the PTP family. The lower k_{cat} observed for the peptide substrates in this study for VHZ relative to YopH and PTP1B parallels the lower rate reported for VHZ catalysis of pNPP.[11] A thorough search for substrate sequences with particularly strong affinity for VHZ is beyond the scope of this study.

The apparent disagreement between our assay results and those of previous reports of VHZ as a DSP led us to consider potential explanations. In one of the previous reports, a commercial kit was used to estimate the phosphatase activity.[10] Our previous experiments with commercial kits based on malachite green assays have shown a tendency to give false positives with some proteins, depending on the quantity of protein used. In these cases, addition of the acidic malachite green solution causes protein precipitation, forming turbidity that is not always visible to the naked eye in the darkly colored solution. The resulting light scattering can register as absorbance over the blank where no protein is added. We avoided this problem by digesting the enzyme with a phosphate-free protease prior to adding the malachite green solution.

In another study, MBP (myelin basic protein) phosphorylated by protein kinase A (PKA) was used in a dephosphorylation assay that followed radioactively labeled phosphate release.[9] The reported pS/pT dephosphorylation (0.0073 pmol/μg) was 1500 times lower than the pY hydrolysis rate (11 pmol/μg). Despite the fact that serine and threonine are the predominant phosphorylation sites, the PKA phosphorylation of MBP is not 100% specific and produces detectable quantities of pY in addition to pS and pT.[42] A low level of incorporation of phosphotyrosine into MBP may explain the low activity of VHZ detected with this substrate.

Finally, the VHZ used in these previous reports contained an N-terminal GST tag. The N-terminal region in classical PTPs contains an important substrate recognition loop. The GST tag alone showed no phosphatase activity, but its proximity to the active site may affect substrate specificity. To avoid potential complications with N-terminal tags, all experiments in the present study used untagged VHZ.

Is the IPD-Loop of VHZ Mobile? The mobility of the WPD-loop in classical PTPs has been extensively documented.[8,43−47] In solution, the loop is dynamic, and substrate−oxyanion binding shifts the equilibrium to favor the closed conformation that brings the general acid into a position favorable for catalysis.[8,48] The crystal structure of the VHZ−VO_3 complex shows the IPD-loop is properly positioned for catalysis and superimposes with the closed WPD-loop conformation observed in classical PTPs. Because the highly conserved W residue is important for WPD-loop dynamics,[49] we searched for related proteins containing substitutions for W in this position. Like VHZ, most of the sequences resulting from this search (Figure 1SC of the Supporting Information) contain isoleucine. Two of these proteins, the *S. solfataricus* PTP and the CDC14B PTP (containing an IPD-loop and FAD-loop, respectively), have been crystallized in both apo (PDB entries 2I6I and 1OHC, respectively) and tungstate-bound forms (PDB entries 2I6M and 1OHD, respectively). These structures reveal no difference in the loop position in ligand-free and ligand-bound forms, which contrasts with the case for classical PTPs. Additionally, the crystal structures of Phytase (PDB entries 2PS2 and 3D1H) obtained with no ligand bound have the identical closed loop position. These findings suggest the general acid loop is not a mobile element in these enzymes. To seek a further rationale for the apparent single conformation of the IPD-loop in VHZ, we aligned the VHZ−VO_3 complex with the YopH WT ligand-free structure (PDB entry 1YPT) where the loop occupies its open conformation. The alignment revealed that, were the IPD-loop of VHZ to adopt an open conformation, D65 would clash with the anionic side chain of E44, which corresponds to the smaller and neutral S287 in YopH (Figure 2S of the Supporting Information). The *S. solfataricus* PTP and Phytase contain analogous E37 and E132 residues in this location. In all, there is no evidence or likelihood that these enzymes undergo conformational changes in their general acid loop. We conclude that, although VHZ is likely related to the classical PTPs in other structural aspects and in substrate preference, its IPD-loop probably does not undergo conformational changes in the process of catalysis.

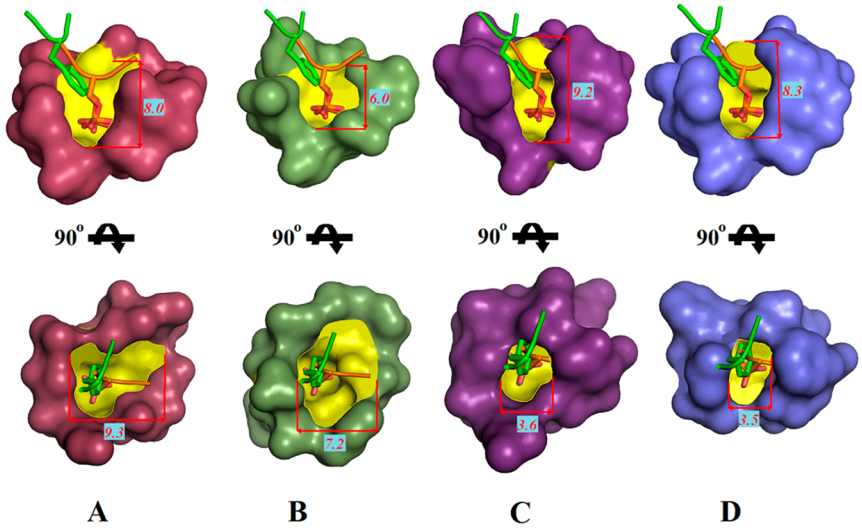

Figure 5. Effect of active site width and depth, which explains the substrate selectivity observed in different PTP subfamilies exemplified by (A) CDC14B (DSP), (B) VHR (DSP), (C) YopH (PTP), and (D) VHZ (blue). The active site dimensions are presented in angstroms. Phosphoserine-containing (orange) and phosphotyrosine-containing (green) peptides are modeled in the active sites so that the P-loop-stabilized phosphate moiety is in catalytic proximity of the nucleophilic cysteine, and the scissile bridging oxygen on the leaving group is within hydrogen bonding distance of the catalytic general acid. The importance of the active site depth for substrate selectivity is illustrated in the top row, whereas the bottom row reveals the effect of the width. The backbone of the phosphoserine-containing peptide in panels C and D is buried below the protein surface, indicating it clashes with several residues on the edge of the active site. At the same time, the binding of the phosphotyrosine-containing peptide reveals no such problem caused by the longer side chain. The importance of this clash for the substrate selectivity is consistent with the reported ability of classical enzymes to catalyze monomeric alkyl phosphate esters, but not when they are part of a peptide.[50]

Shape of the Active Site. The active site width and depth are primary factors defining substrate specificity in the PTP family. In Figure 5, the active sites of two DSPs [CDC14B (A) and VHR (B)], the classical PTP YopH (C), and VHZ (D) are rendered as surface models. Two peptide substrates containing pY and pS are modeled in the catalytically favorable orientation. In this position, the equatorial oxygens are stabilized by hydrogen bonds from the P-loop, and the scissile phosphate monoester oxygen is located within hydrogen bond distance of the general acid. These common determinants allow one to model substrates into the active sites of PTPs and DSPs with little ambiguity. Atypical DSPs are characterized by shallow and/or broad active sites that allow them to accommodate the aliphatic side chains of pS (2.63 Å distance between phosphorus and the α-carbon) and pT (3.76 Å), in addition to longer pY (7.44 Å) residues (Figure 5A,B). In contrast, classical PTPs have a deep and narrow active site pocket that accommodates pY-containing peptides (Figure 5C,D). Modeling shows that the pT and pS side chains of a polypeptide substrate are too short to reach the nucleophilic cysteine at the bottom of the active site, consistent with their lack of activity by classical PTPs, although low activity with monomeric alkyl phosphate esters has been reported.[50] With its shallower active site depth of 6 Å, the DSP VHR already displays a 2000-fold preference for pY- over pS/pT-containing substrates. The active site of VHZ is deeper than that of VHR and is close to those of classical tyrosine-specific PTPs (Figure 5B–D). The depth of the active site is a required but not exclusive factor that provides PTPs with the ability to discriminate between aliphatic and aromatic substrates. For example, CDC14B reveals a deep 8 Å active site crevice but specifically targets cyclin-dependent kinases phosphorylated on serine.[51] This ability is provided by the greater width of its active site, which renders dual specificity to some enzymes in the family. The active site of VHZ is both narrow and deep, similar to those of classical PTPs. This provides a structural rationale for the absence of activity toward pS- and pT-containing peptides observed in the substrate screen.

In conclusion, a new structure of VHZ complexed with the physiologically relevant inhibitor vanadate has been determined. This structure reveals important evidence that, together with the results of broad phosphopeptide screening, allows the following conclusions to be reached. (a) VHZ is a viable catalyst for the hydrolysis of pY-containing peptides. In contrast, no activity toward pS or pT-containing peptides was observed. This tendency is that of a classical PTP rather than a DSP. (b) Classical PTPs have a deep and narrow active site cavity consistent with the observed specificity for pY-containing substrates. Atypical DSPs have a broader and shallower active site to accommodate phosphoserine/threonine side chains. The active site of VHZ more closely resembles those of classical PTPs. (c) VHZ lacks the secondary positively charged binding site characteristic of atypical DSPs that confers a preference for bisphosphorylated substrates.[30] A conserved arginine residue characterizes this binding site. A corresponding R129 residue in VHZ is in a position analogous to that of the secondary binding pockets of atypical DSPs,[30] but it is blocked from the surface by the N7 side chain. (d) In classical PTPs, a structural water molecule seen in crystal structures stabilizes the position of the general acid loop. No such water molecule is observed in DSP structures, where this structural role is filled by the asparagine residue from the N-loop and a serine residue from the P-loop. As a result of differences in the positioning of the general acid loop, protonation of the leaving group occurs from different angles. In both respects, VHZ resembles PTPs rather than DSPs. (e) The Q-loop motif containing two catalytically important glutamines (QXXXQ) is present in all classical PTPs. Atypical DSPs contain the N-loop in the analogous position. Its conserved PNXXF motif stabilizes the general acid and defines the wide and shallow active site of atypical DSPs. Analogous to the classical PTPs, the Q-loop in VHZ contains E134 and Q138 residues that can be

superimposed with Q446 and Q450 in YopH. We conclude that the Q-loop in VHZ operates as in classical PTPs.

While sharing a number of similarities, VHZ also bears several important distinctions from the classical PTPs. (a) In addition to the catalytic domain, classical PTPs contain multiple domains defining substrate specificity and subcellular localization. The VHZ protein is comprised of only a catalytic domain and lacks the N-terminal extension containing a substrate recognition loop found in all classical PTPs.[26,52] (b) The general acid IPD-loop in VHZ, unlike the WPD-loop in classical PTPs, is not mobile.

In total, the data suggest that VHZ does not fit the profile of an atypical DSP but rather is structurally and functionally more closely related to tyrosine-specific PTPs. However, the absence of a substrate recognition loop and additional domains is not consistent with its placement as either a receptor or nonreceptor type classical PTP. It is similar in size to the class II low-molecular weight (LMW) phosphatases that display the same phosphotyrosine specificity; however, significant sequence, functional, and structural distinctions exist between the LMW family and VHZ.[53,54] We propose that a separate category designated "atypical PTPs", shown in the shaded box in Figure 6, is more appropriate for VHZ. Other analogous phosphatases, including that from *S. solfataricus*, and others identified in section C of Figure 1S of the Supporting Information may also prove to belong in this category.

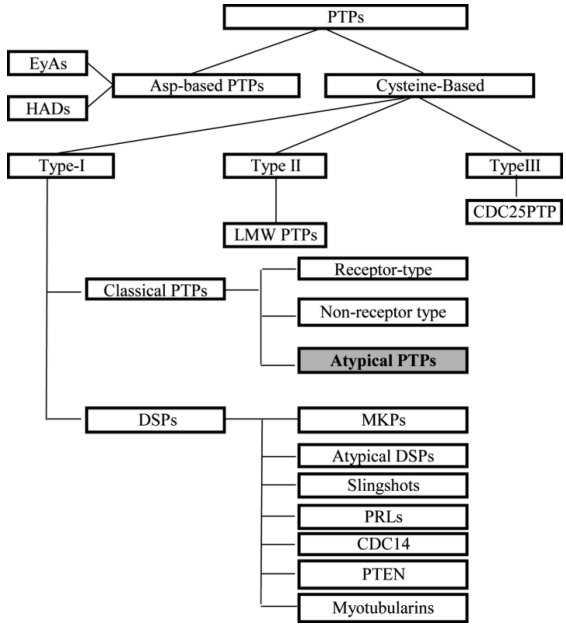

Figure 6. Classification of PTP family members.[1] On the basis of early reports, VHZ has been suggested to belong to the atypical DSP group. The evidence reported here suggests VHZ is structurally and functionally more closely related to classical tyrosine-specific PTPs. However, the absence of a substrate recognition loop and additional domains is not consistent with its placement as either a receptor or nonreceptor type classical PTP. We propose that a separate category designated atypical PTPs, shown in the shaded box, is more appropriate for VHZ and probably for similar enzymes in Figure 1S of the Supporting Information.

PTPs are classified on the basis of sequence similarity and substrate specificity, as well as protein size and subcellular localization. Structural and functional distinctions between classical PTPs and atypical PTPs can be used to discriminate between the two subfamilies. The identification and proper classification of VHZ will assist in the subsequent research into its biological role and its physiological substrates.

■ ASSOCIATED CONTENT

Supporting Information

Complete list of phosphorylated peptides in the substrate screen; phosphopeptides that showed the highest percentage of phosphate release by VHZ; partial sequence alignment of residues 63−138 of VHZ with classic PTPs, DSPs, and other PTPs containing the XXDXXXP sequence of the general acid loop and structurally related to VHZ; and a structural alignment of the VHZ−vanadate complex with YopH. This material is available free of charge via the Internet at http://pubs.acs.org.

■ AUTHOR INFORMATION

Corresponding Author

*A.C.H.: e-mail, alvan.hengge@usu.edu; phone, (435) 797-3442; fax, (435) 797-3390. S.J.J.: e-mail, sean.johnson@usu.edu; telephone, (435) 797-2089; fax, (435) 797-3390.

Funding

This work was supported by National Institutes of Health Grant GM47297 (A.C.H.).

Notes

The authors declare no competing financial interest.

■ ABBREVIATIONS

DSP, dual-specificity phosphatase; PTP, protein tyrosine phosphatase; VHZ, VH1-related member Z; VHR, VH1-related member R; YopH, *Yersinia* outer protein H; VSP, voltage sensor (sensing) protein; PTEN, phosphatase and tensin homologue; KAP1, kinase- associated phosphatase; PhyA, phytase A; SsoPTP, *S. solfataricus* protein tyrosine phosphatase; TEV protease, tobacco etch virus protease; MBP, myelin basic protein; PKA, protein kinase A; MAPK, mitogen-activated protein kinase; ERK, extracellular signal-regulated kinase; JNK, c-Jun N-terminal.

■ REFERENCES

(1) Alonso, A., Sasin, J., Bottini, N., Friedberg, I., Osterman, A., Godzik, A., Hunter, T., Dixon, J., and Mustelin, T. (2004) Protein tyrosine phosphatases in the human genome. *Cell 117*, 699−711.

(2) Hunter, T. (1995) Protein kinases and phosphatases: The yin and yang of protein phosphorylation and signaling. *Cell 80*, 225−236.

(3) Cleland, W. W., and Hengge, A. C. (2006) Enzymatic mechanisms of phosphate and sulfate transfer. *Chem. Rev. 106*, 3252−3278.

(4) Jackson, M. D., and Denu, J. M. (2001) Molecular reactions of protein phosphatases: Insights from structure and chemistry. *Chem. Rev. 101*, 2313−2340.

(5) Denu, J. M., Stuckey, J. A., Saper, M. A., and Dixon, J. E. (1996) Form and function in protein dephosphorylation. *Cell 87*, 361−364.

(6) Patterson, K. I., Brummer, T., O'Brien, P. M., and Daly, R. J. (2009) Dual-specificity phosphatases: Critical regulators with diverse cellular targets. *Biochem. J. 418*, 475−489.

(7) Bayón, Y., and Alonso, A. (2010) Atypical DUSPs: 19 phosphatases in search of a role. *Emerging Signaling Pathways in Tumor Biology*, 185−208.

(8) Schubert, H. L., Fauman, E. B., Stuckey, J. A., Dixon, J. E., and Saper, M. A. (1995) A ligand-induced conformational change in the *Yersinia* protein tyrosine phosphatase. *Protein Sci. 4*, 1904−1913.

(9) Takagaki, K., Satoh, T., Tanuma, N., Masuda, K., Takekawa, M., Shima, H., and Kikuchi, K. (2004) Characterization of a novel low-molecular-mass dual-specificity phosphatase-3 (LDP-3) that enhances activation of JNK and p38. *Biochem. J. 383*, 447−455.

(10) Wu, Q., Li, Y., Gu, S., Li, N., Zheng, D., Li, D., Zheng, Z., Ji, C., Xie, Y., and Mao, Y. (2004) Molecular cloning and characterization of a novel dual-specificity phosphatase 23 gene from human fetal brain. *Int. J. Biochem. Cell Biol. 36*, 1542−1553.
(11) Alonso, A., Burkhalter, S., Sasin, J., Tautz, L., Bogetz, J., Huynh, H., Bremer, M. C., Holsinger, L. J., Godzik, A., and Mustelin, T. (2004) The minimal essential core of a cysteine-based protein-tyrosine phosphatase revealed by a novel 16-kDa VH1-like phosphatase, VHZ. *J. Biol. Chem. 279*, 35768−35774.
(12) Rahmouni, S., Cerignoli, F., Alonso, A., Tsutji, T., Henkens, R., Zhu, C., Louis-dit-Sully, C., Moutschen, M., Jiang, W., and Mustelin, T. (2006) Loss of the VHR dual-specific phosphatase causes cell-cycle arrest and senescence. *Nat. Cell Biol. 8*, 524−531.
(13) Camps, M., Nichols, A., and Arkinstall, S. (2000) Dual specificity phosphatases: A gene family for control of MAP kinase function. *FASEB J. 14*, 6−16.
(14) Henkens, R., Delvenne, P., Arafa, M., Moutschen, M., Zeddou, M., Tautz, L., Boniver, J., Mustelin, T., and Rahmouni, S. (2008) Cervix carcinoma is associated with an up-regulation and nuclear localization of the dual-specificity protein phosphatase VHR. *BMC Cancer 8*, 147.
(15) Kim, J.-H., and Jeong, D.-G. (2007) Proteomic Identification of Proteins Interacting with a Dual Specificity Protein Phosphatase, VHZ. *J. Appl. Biol. Chem. 50*, 58−62.
(16) Wu, L., and Zhang, Z. Y. (1996) Probing the function of Asp128 in the lower molecular weight protein-tyrosine phosphatase-catalyzed reaction. A pre-steady-state and steady-state kinetic investigation. *Biochemistry 35*, 5426−5434.
(17) Tang, J. P., Tan, C. P., Li, J., Chan, S. W., Huang, Z. Y., Li, W. C., Chen, J., and Zeng, Q. (2010) VHZ is a novel centrosomal phosphatase associated with cell growth and human primary cancers. *Mol. Cancer 9*, 128.
(18) Agarwal, R., Burley, S. K., and Swaminathan, S. (2008) Structure of human dual specificity protein phosphatase 23, VHZ, enzyme-substrate/product complex. *J. Biol. Chem. 283*, 8946−8953.
(19) Polayes, D. A., Goldstein, A., Ward, G., and Hughes, A. J. (1994) TEV protease, recombinant: A site-specific protease for efficient cleavage of affinity tags from expressed proteins. *Focus 16*, 4−7.
(20) Qi, D., and Scholthof, K. B. (2008) A one-step PCR-based method for rapid and efficient site-directed fragment deletion, insertion, and substitution mutagenesis. *J. Virol. Methods 149*, 85−90.
(21) Gordon, J. A. (1991) Use of vanadate as protein-phosphotyrosine phosphatase inhibitor. *Methods Enzymol. 201*, 477−482.
(22) Adams, P. D., Afonine, P. V., Bunkoczi, G., Chen, V. B., Davis, I. W., Echols, N., Headd, J. J., Hung, L. W., Kapral, G. J., Grosse-Kunstleve, R. W., McCoy, A. J., Moriarty, N. W., Oeffner, R., Read, R. J., Richardson, D. C., Richardson, J. S., Terwilliger, T. C., and Zwart, P. H. (2010) PHENIX: A comprehensive Python-based system for macromolecular structure solution. *Acta Crystallogr. D66*, 213−221.
(23) Emsley, P., Lohkamp, B., Scott, W. G., and Cowtan, K. (2010) Features and Development of Coot. *Acta Crystallogr. D66*, 486−501.
(24) Davis, I. W., Murray, L. W., Richardson, J. S., and Richardson, D. C. (2004) MolProbity: Structure validation and all-atom contact analysis for nucleic acids and their complexes. *Nucleic Acids Res. 32*, 615−619.
(25) *The PyMOL Molecular Graphics System*, version 1.5.0.1 Schrödinger, LLC.
(26) Sarmiento, M., Puius, Y. A., Vetter, S. W., Keng, Y. F., Wu, L., Zhao, Y., Lawrence, D. S., Almo, S. C., and Zhang, Z. Y. (2000) Structural basis of plasticity in protein tyrosine phosphatase 1B substrate recognition. *Biochemistry 39*, 8171−8179.
(27) Kuznetsov, V. I., Alexandrova, A. N., and Hengge, A. C. (2012) Metavanadate at the active site of the phosphatase VHZ. *J. Am. Chem. Soc. 134*, 14298−14301.
(28) Zeng, W. Y., Wang, Y. H., Zhang, Y. C., Yang, W. L., and Shi, Y. Y. (2003) Functional significance of conserved glycine 127 in a human dual-specificity protein tyrosine phosphatase. *Biochemistry (Moscow, Russ. Fed.) 68*, 634−638.
(29) Kim, J. H., Shin, D. Y., Han, M. H., and Choi, M. U. (2001) Mutational and kinetic evaluation of conserved His-123 in dual specificity protein-tyrosine phosphatase vaccinia H1-related phosphatase: Participation of Tyr-78 and Thr-73 residues in tuning the orientation of His-123. *J. Biol. Chem. 276*, 27568−27574.
(30) Schumacher, M. A., Todd, J. L., Rice, A. E., Tanner, K. G., and Denu, J. M. (2002) Structural basis for the recognition of a bisphosphorylated MAP kinase peptide by human VHR protein phosphatase. *Biochemistry 41*, 3009−3017.
(31) Brandao, T. A., Hengge, A. C., and Johnson, S. J. (2010) Insights into the reaction of protein tyrosine phosphatase 1B. Crystal structures for transition-state analogs of both catalytic steps. *J. Biol. Chem. 285*, 15874−15883.
(32) Zhao, Y., Wu, L., Noh, S. J., Guan, K. L., and Zhang, Z. Y. (1998) Altering the nucleophile specificity of a protein-tyrosine phosphatase-catalyzed reaction. Probing the function of the invariant glutamine residues. *J. Biol. Chem. 273*, 5484−5492.
(33) Lohse, D. L., Denu, J. M., Santoro, N., and Dixon, J. E. (1997) Roles of aspartic acid-181 and serine-222 in intermediate formation and hydrolysis of the mammalian protein-tyrosine-phosphatase PTP1. *Biochemistry 36*, 4568−4575.
(34) Zhang, Z., Harms, E., and Van Etten, R. L. (1994) Asp129 of low molecular weight protein tyrosine phosphatase is involved in leaving group protonation. *J. Biol. Chem. 269*, 25947−25950.
(35) Brandao, T. A., Robinson, H., Johnson, S. J., and Hengge, A. C. (2009) Impaired acid catalysis by mutation of a protein loop hinge residue in a YopH mutant revealed by crystal structures. *J. Am. Chem. Soc. 131*, 778−786.
(36) Phan, J., Tropea, J. E., and Waugh, D. S. (2007) Structure-assisted discovery of *Variola major* H1 phosphatase inhibitors. *Acta Crystallogr. D63*, 698−704.
(37) Zhou, G., Denu, J. M., Wu, L., and Dixon, J. E. (1994) The catalytic role of Cys124 in the dual specificity phosphatase VHR. *J. Biol. Chem. 269*, 28084−28090.
(38) Zhao, Y., and Zhang, Z. Y. (1996) Reactivity of alcohols toward the phosphoenzyme intermediate in the protein-tyrosine phosphatase-catalyzed reaction: Probing the transition state of the dephosphorylation step. *Biochemistry 35*, 11797−11804.
(39) Zhou, B., and Zhang, Z. Y. (2002) The activity of the extracellular signal-regulated kinase 2 is regulated by differential phosphorylation in the activation loop. *J. Biol. Chem. 277*, 13889−13899.
(40) Denu, J. M., Zhou, G., Wu, L., Zhao, R., Yuvaniyama, J., Saper, M. A., and Dixon, J. E. (1995) The purification and characterization of a human dual-specific protein tyrosine phosphatase. *J. Biol. Chem. 270*, 3796−3803.
(41) Zhang, Z. Y., Maclean, D., McNamara, D. J., Sawyer, T. K., and Dixon, J. E. (1994) Protein tyrosine phosphatase substrate specificity: Size and phosphotyrosine positioning requirements in peptide substrates. *Biochemistry 33*, 2285−2290.
(42) Kishimoto, A., Nishiyama, K., Nakanishi, H., Uratsuji, Y., Nomura, H., Takeyama, Y., and Nishizuka, Y. (1985) Studies on the phosphorylation of myelin basic protein by protein kinase C and adenosine 3′:5′-monophosphate-dependent protein kinase. *J. Biol. Chem. 260*, 12492−12499.
(43) Barford, D., Flint, A. J., and Tonks, N. K. (1994) Crystal structure of human protein tyrosine phosphatase 1B. *Science 263*, 1397−1404.
(44) Stuckey, J. A., Schubert, H. L., Fauman, E. B., Zhang, Z. Y., Dixon, J. E., and Saper, M. A. (1994) Crystal structure of *Yersinia* protein tyrosine phosphatase at 2.5 Å and the complex with tungstate. *Nature 370*, 571−575.
(45) Ala, P. J., Gonneville, L., Hillman, M. C., Becker-Pasha, M., Wei, M., Reid, B. G., Klabe, R., Yue, E. W., Wayland, B., Douty, B., Polam, P., Wasserman, Z., Bower, M., Combs, A. P., Burn, T. C., Hollis, G. F., and Wynn, R. (2006) Structural basis for inhibition of protein-tyrosine phosphatase 1B by isothiazolidinone heterocyclic phosphonate mimetics. *J. Biol. Chem. 281*, 32784−32795.
(46) Khajehpour, M., Wu, L., Liu, S., Zhadin, N., Zhang, Z. Y., and Callender, R. (2007) Loop dynamics and ligand binding kinetics in the reaction catalyzed by the *Yersinia* protein tyrosine phosphatase. *Biochemistry 46*, 4370−4378.

(47) Wang, F., Li, W., Emmett, M. R., Hendrickson, C. L., Marshall, A. G., Zhang, Y. L., Wu, L., and Zhang, Z. Y. (1998) Conformational and dynamic changes of *Yersinia* protein tyrosine phosphatase induced by ligand binding and active site mutation and revealed by H/D exchange and electrospray ionization Fourier transform ion cyclotron resonance mass spectrometry. *Biochemistry 37*, 15289−15299.
(48) Fauman, E. B., Yuvaniyama, C., Schubert, H. L., Stuckey, J. A., and Saper, M. A. (1996) The X-ray crystal structures of *Yersinia* tyrosine phosphatase with bound tungstate and nitrate. Mechanistic implications. *J. Biol. Chem. 271*, 18780−18788.
(49) Brandao, T. A., Johnson, S. J., and Hengge, A. C. (2012) The molecular details of WPD-loop movement differ in the protein-tyrosine phosphatases YopH and PTP1B. *Arch. Biochem. Biophys. 525*, 53−59.
(50) Zhang, Z. Y. (1995) Are protein-tyrosine phosphatases specific for phosphotyrosine? *J. Biol. Chem. 270*, 16052−16055.
(51) Bremmer, S. C., Hall, H., Martinez, J. S., Eissler, C. L., Hinrichsen, T. H., Rossie, S., Parker, L. L., Hall, M. C., and Charbonneau, H. (2012) Cdc14 Phosphatases Preferentially Dephosphorylate a Subset of Cyclin-dependent kinase (Cdk) Sites Containing Phosphoserine. *J. Biol. Chem. 287*, 1662−1669.
(52) Sarmiento, M., Zhao, Y., Gordon, S. J., and Zhang, Z. Y. (1998) Molecular basis for substrate specificity of protein-tyrosine phosphatase 1B. *J. Biol. Chem. 273*, 26368−26374.
(53) Ramponi, G., and Stefani, M. (1997) Structure and function of the low Mr phosphotyrosine protein phosphatases. *Biochim. Biophys. Acta 1341*, 137−156.
(54) Raugei, G., Ramponi, G., and Chiarugi, P. (2002) Low molecular weight protein tyrosine phosphatases: Small, but smart. *Cell. Mol. Life Sci. 59*, 941−949.